SDSS IV MaNGA: Discovery of an Hα Blob Associated with a Dry Galaxy Pair—Ejected Gas or a "Dark" Galaxy Candidate?

Lihwai Lin[1], Jing-Hua Lin[1,2], Chin-Hao Hsu[1,2], Hai Fu[3], Song Huang[4], Sebastián F. Sánchez[5], Stephen Gwyn[6],
Joseph D. Gelfand[7,8], Edmond Cheung[4], Karen Masters[9], Sébastien Peirani[4,10], Wiphu Rujopakarn[4,11], David V. Stark[4],
Francesco Belfiore[12,13], M. S. Bothwell[12,13], Kevin Bundy[4,14], Alex Hagen[15,16], Lei Hao[17], Shan Huang[8], David Law[18],
Cheng Li[19], Chris Lintott[20], Roberto Maiolino[12,13], Alexandre Roman-Lopes[21], Wei-Hao Wang[1], Ting Xiao[17], Fangting Yuan[17],
Dmitry Bizyaev[22,23], Elena Malanushenko[22], Niv Drory[24], J. G. Fernández-Trincado[25], Zach Pace[26], Kaike Pan[22], and
Daniel Thomas[9]

[1] Institute of Astronomy & Astrophysics, Academia Sinica, Taipei 10617, Taiwan; lihwailin@asiaa.sinica.edu.tw
[2] Department of Physics, National Taiwan University, 10617, Taipei, Taiwan
[3] Department of Physics & Astronomy, University of Iowa, Iowa City, IA 52242, USA
[4] Kavli Institute for the Physics and Mathematics of the Universe (WPI), The University of Tokyo Institutes for Advanced Study, The University of Tokyo, Kashiwa, Chiba 277-8583, Japan
[5] Instituto de Astronomía, Universidad Nacional Autónoma de Mexico, A.P. 70-264, 04510, México, D.F., Mexico
[6] NRC-Herzberg Astronomy and Astrophysics, National Research Council of Canada, 5071 West Saanich Road, Victoria, British Columbia V9E 2E7, Canada
[7] NYU Abu Dhabi, P.O. Box 129188, Abu Dhabi, UAE
[8] Center for Cosmology and Particle Physics, New York University, New York, NY 10003, USA
[9] Institute of Cosmology & Gravitation, University of Portsmouth, Dennis Sciama Building, Portsmouth, PO1 3FX, UK
[10] Institut d'Astrophysique de Paris (UMR 7095: CNRS & UPMC), 98 bis Boulevard Arago, F-75014 Paris, France
[11] Department of Physics, Faculty of Science, Chulalongkorn University, 254 Phayathai Road, Pathumwan, Bangkok 10330, Thailand
[12] Cavendish Laboratory, University of Cambridge, 19 J. J. Thomson Avenue, Cambridge CB3 0HE, UK
[13] University of Cambridge, Kavli Institute for Cosmology, Cambridge, CB3 0HE, UK
[14] UCO/Lick Observatory, University of California, Santa Cruz, 1156 High Street, Santa Cruz, CA 95064, USA
[15] Dept. of Astronomy & Astrophysics, Pennsylvania State University, University Park, PA 16802, USA
[16] Institute for Gravitation and the Cosmos, Pennsylvania State University, University Park, PA 16802, USA
[17] Shanghai Astronomical Observatory, Chinese Academy of Science, 80 Nandan Road, Shanghai 200030, China
[18] Space Telescope Science Institute, 3700 San Martin Drive, Baltimore, MD 21218, USA
[19] Tsinghua Center of Astrophysics & Department of Physics, Tsinghua University, Beijing 100084, China
[20] Sub-department of Astrophysics, Department of Physics, University of Oxford, Denys Wilkinson Building, Keble Road, Oxford OX1 3RH, UK
[21] Departamento de Fisica, Facultad de Ciencias, Universidad de La Serena, Cisternas 1200, La Serena, Chile
[22] Apache Point Observatory and New Mexico State University, P.O. Box 59, Sunspot, NM, 88349-0059, USA
[23] Sternberg Astronomical Institute, Moscow State University, Moscow, Russia
[24] McDonald Observatory, The University of Texas at Austin, 1 University Station, Austin, TX 78712, USA
[25] Institut Utinam, CNRS UMR 6213, Université de Franche-Comté, OSU THETA Franche-Comté-Bourgogne, Observatoire de Besançon, BP 1615, 25010 Besançon Cedex, France
[26] Department of Astronomy, University of Wisconsin-Madison, 475 N. Charter Street, Madison WI 53703, USA

Abstract

We report the discovery of a mysterious giant Hα blob that is ∼8 kpc away from the main MaNGA target 1-24145, one component of a dry galaxy merger, and has been identified in the first-year SDSS-IV MaNGA data. The size of the Hα blob is ∼3–4 kpc in radius, and the Hα distribution is centrally concentrated. However, there is no optical continuum counterpart in the deep broadband images reaching ∼26.9 mag arcsec^{-2} in surface brightness. We estimate that the masses of the ionized and cold gases are $3.3 \times 10^5 \, M_\odot$ and $<1.3 \times 10^9 \, M_\odot$, respectively. The emission-line ratios indicate that the Hα blob is photoionized by a combination of massive young stars and AGNs. Furthermore, the ionization line ratio decreases from MaNGA 1-24145 to the Hα blob, suggesting that the primary ionizing source may come from MaNGA 1-24145, likely a low-activity AGN. Possible explanations for this Hα blob include the AGN outflow, the gas remnant being tidally or ram-pressure stripped from MaNGA 1-24145, or an extremely low surface brightness galaxy. However, the stripping scenario is less favored according to galaxy merger simulations and the morphology of the Hα blob. With the current data, we cannot distinguish whether this Hα blob is ejected gas due to a past AGN outburst, or a special category of "ultra-diffuse galaxy" interacting with MaNGA 1-24145 that further induces the gas inflow to fuel the AGN in MaNGA 1-24145.

Key words: galaxies: evolution – galaxies: interactions – galaxies: peculiar

1. Introduction

It is known that the observed number density of the satellite galaxies in the Local Group and our own Milky Way is orders of magnitude lower than the predictions from cosmological simulations, i.e., the so-called "missing satellite problem" (Klypin et al. 1999; Moore et al. 1999). One popular explanation for this problem is that low-mass halos fail to form stars efficiently, such that they are below the detection limit of most imaging surveys. Under this paradigm, "dark" galaxies are gas-rich galaxies that do not emit sufficient optical light due to their low efficiency in forming stars, but they are thought to be the building blocks of normal star-forming galaxies. This type of galaxy is an ideal laboratory to study early stages of star formation, which

could lead to the understanding of how the star formation is triggered.

In general it is very difficult to identify dark galaxies since they are extremely faint in the optical. To date, very few dark candidates have been identified and confirmed. The Arecibo Legacy Fast ALFA (ALFALFA) H I survey (Giovanelli et al. 2005) has discovered on the order of ~200 H I sources not associated with apparent optical counterparts, however, most of them are likely to have tidal origins (Haynes et al. 2011). A pilot study suggested that none of the remaining objects they have explored are dark galaxies, after cross-checking with data in other wavelengths (Cannon et al. 2015).

Recently, van Dokkum et al. (2015) have identified a new class of low surface brightness (LSB) dwarf galaxies in the Coma cluster, often referred to as "ultra-diffuse" galaxies (UDGs), using the Dragonfly Telescope Array (Abraham & van Dokkum 2014). These UDGs not only have a LSB (24–26 mag arcsec^{-2}), but also show extended structures with a size comparable to L^* galaxies. Although these UDGs are found in special environments and may not necessarily represent the global dwarf population, the discovery of this type of galaxy suggests we might have missed numerous faint dwarfs due to observation limitations in the past.

In addition to the aforementioned efforts, the optical Integral Field Unit (IFU) observations open a plausible window into probing the dwarf populations. Normally, emission lines ionized by star-forming regions, AGNs, or shocks are stronger than the stellar continuum and hence, can be easily detected with a reasonable integration time. With the large area covered by IFU, the structures of ionized gas can be probed out to several tens of kiloparsecs. Isolated ionized gases that are separate from a nearby galaxy or a quasar have been readily studied in the IFU as well as in spectroscopic observations (Fu & Stockton 2007a, 2007b, 2008; Lintott et al. 2009; Husemann et al. 2010; Keel et al. 2012; Hamer et al. 2012; Cheung et al. 2016b). Although the majority of those ionized gases are suggested or inferred to have external origins, such as gas accretion, cooling of ICM, or minor mergers, their nature remains unknown.

Here we report the discovery of a giant Hα blob that does not have any optical counterparts in the deep CFHT *gri* images. However, the morphology and emission line analyses suggest that it could either be ejected gas due to past AGN activity or, it could be a special type of UDG (or "dark" galaxy). In Section 2, we describe the multiwavelength data for this system. We present the main results in Section 3. Section 4 discusses the plausible origins of this system and the important implications of our results. Conclusions are given in Section 5. Throughout this paper we adopt the following cosmology: $H_0 = 100\, h\,\mathrm{km\,s^{-1}\,Mpc^{-1}}$, $\Omega_m = 0.3$, and $\Omega_\Lambda = 0.7$. We use a Salpeter IMF when deriving the star formation rate (SFR) from various observables and we adopt the Hubble constant $h = 0.7$ when calculating rest-frame magnitudes. All the magnitudes are given in the AB system.

2. Data

2.1. Optical Integral Field Data

This system, MaNGA 1-24145 ($z = 0.0322$, R.A. = 258.84693, decl. = 57.43288, $M_* \sim 10^{11}\ M_\odot$[27]), was

---

[27] Based on the NASA-Sloan Atlas catalog: http://www.nsatlas.org.

observed in the first 1392 galaxies as part of the ongoing SDSS-IV/MaNGA survey (Bundy et al. 2015; Drory et al. 2015; Law et al. 2016; SDSS Collaboration et al. 2016; Yan et al. 2016a, 2016b). MaNGA is an IFU survey of 10,000 nearby galaxies with a spectral resolution varying from $R \sim 1400$ at 4000 Å to $R \sim 2600$ at 9000 Å. The survey uses the BOSS spectrographs (Smee et al. 2013) on the 2.5 m Sloan Foundation Telescope (Gunn et al. 2006). The median full width at half maximum of the MaNGA point spread function (PSF) of the datacube is ~2″.5. The MaNGA data used were reduced using the MPL-4 version of the MaNGA data reduction pipeline (Law et al. 2016). The spectral line fitting is carried out using Pipe3D pipeline (Sánchez et al. 2016a). The stellar continuum was first modeled with a linear combination of 12 single stellar population (SSP) templates that were extracted from the MILES project (Sánchez-Blázquez et al. 2006; Vazdekis et al. 2010; Falcón-Barroso et al. 2011). The best-fit stellar continuum is then subtracted from the reduced data spectrum for the emission line measurements. Details of the fitting procedures are described in Sánchez et al. (2016b). To ensure that reliable measurements are obtained, we restrict our analysis to spaxels where the error-to-flux ratio of the line fitting is less than 1 in subsequent analyses.

To correct for dust reddening, we follow the method described in the Appendix of Vogt et al. (2013) to compute the reddening correction using the Balmer decrement at each spaxel of the IFU cube. An extinction law with $Rv = 4.5$ (Fischera & Dopita 2005) is used. The SFR is then estimated based on this extinction-corrected Hα flux.

Figure 1 shows the SDSS *gri* composite image (left panel), and the Hα flux map (right panel) of this system (MaNGA 1-24145). The SDSS image indicates that MaNGA 1-24145 (nicknamed "Satsuki") has a companion galaxy (nicknamed "Mei") located in the lower left of MaNGA 1-24145. The stellar absorption lines suggest that these two galaxies are at similar redshifts, with the line of sight velocities differing by ~200 km s^{-1}. In addition, both galaxies are round and red according to the SDSS images. Therefore, these two galaxies likely form a dry (gas-poor) merger system. The compact source in the upper-left corner of the image is a foreground star according to the MaNGA spectrum, and hence it is irrelevant to the dry merger system we are probing for in this work.

What is striking about this system is that in the upper-right corner of the Hα map, a giant Hα blob exists (R.A. = 258.84314; decl. = 57.43529), however, it does not have any optical counterpart in the SDSS images. The size of the Hα blob is ~3.2 kpc in radius. This Hα blob (nicknamed "Totoro") is 7.7 kpc away from Satsuki, and is connected to the Hα emission of Satsuki through tail-like structures. To ensure that the Hα emission at the position of Totoro is not due to artifacts in the data, we check the MaNGA spectra at various spaxels in the region of Totoro. We found that multiple emission lines, including Hα, [N II] 6584, [S II] 6717,6731, and [O III] 5007 lines are clearly detected in those regions, suggesting that the Hα blob is a real feature. Figure 2 displays the reconstructed *ugr* image from the MaNGA continuum (left panel) and the [O III] + Hα+ [N II] composite image (right panel). It can be seen that the reconstructed continuum map from the MaNGA data is as smooth as SDSS. The three upper panels of Figure 3 show the MaNGA spectra of the central pixels for Satsuki, Mei, and Totoro, respectively. The two elliptical galaxies are mainly composed of old stellar
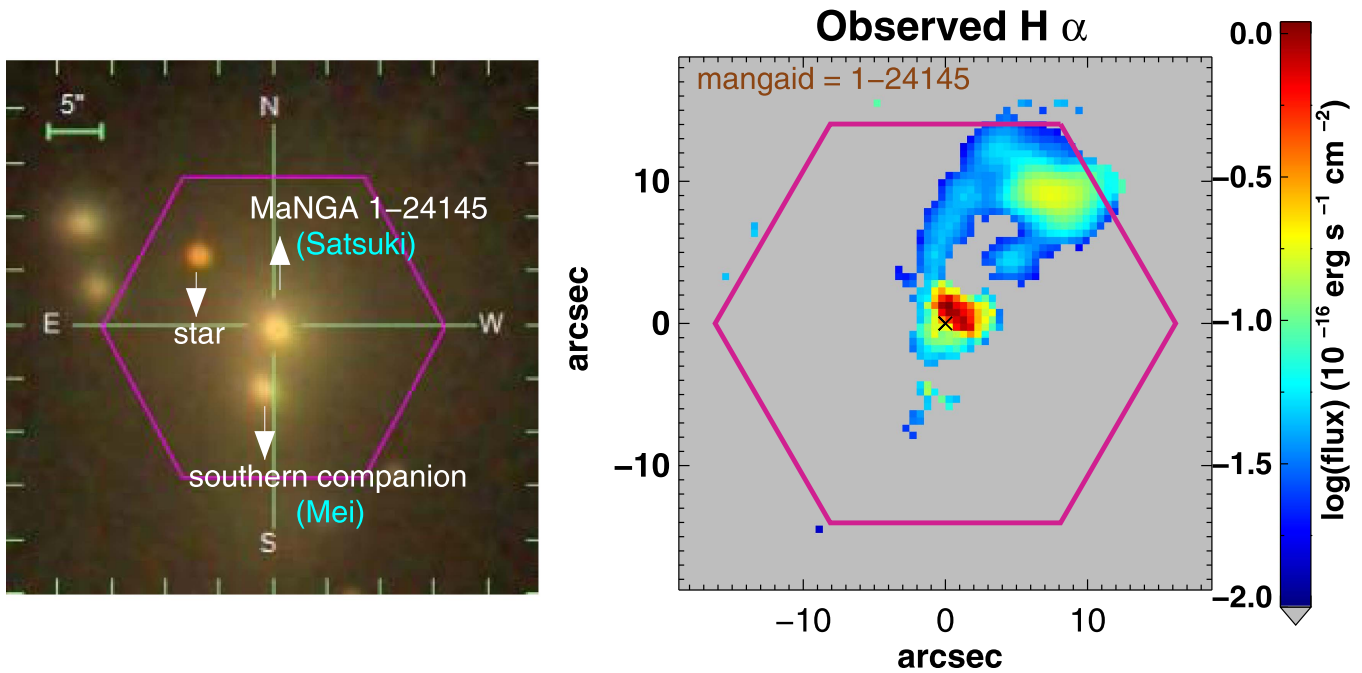
Figure 1. Left: the SDSS *gri* composite image of MaNGA 1-24145 with the MaNGA hexagonal bundle field of view (FoV) overlaid. This system was observed with the 127 fiber bundle of MaNGA, so this hexagon is ~32″5 in diameter. The data extend to regions just outside the hexagon because of the dithering. Three distinct objects are visible within the bundle, including two elliptical galaxies (Satsuki and Mei) and one foreground star. Right: the observed Hα flux map from the MaNGA observations.
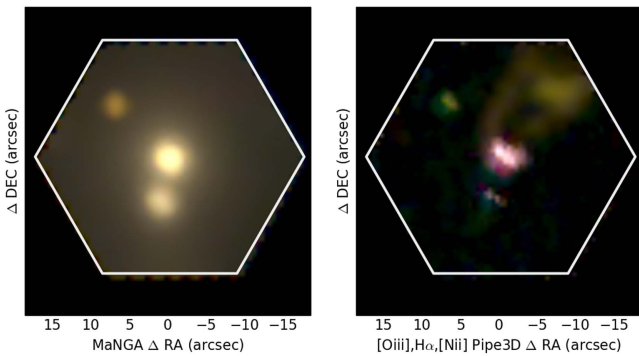
Figure 2. Left: the *ugi* composite image reconstructed using the MaNGA continuum with the MaNGA hexagonal bundle field of view (FoV) overlaid. Right: the [O III]+Hα+[N II] composite image. The flux scales of the three lines are adjusted in order to highlight the Hα blob. In both panels, the *x*- and *y*-axes have the same scale.

populations, consistent with the morphology classification of being early-type galaxies (ETGs), whereas the blob is dominated by emission lines.

2.2. Optical Imaging Data

The imaging data come from two sources: the DR12 release of the SDSS photometric survey (York et al. 2000), which reaches *r* ~ 22, and deeper observations with CFHT/Mega-Cam in *g*, *r*, and *i*. The latter combines archival data downloaded from the CADC server and the data taken in 2015 summer (PI: Lihwai Lin) with the Director Discretionary time program. All the MegaCam data were processed and stacked via MegaPipe (Gwyn 2008). The final images have a 5σ limiting mag of 25.7, 26.2, and 25.2 mag (1″ aperture in

radius) and a surface brightness 5σ limit of 26.4, 26.9, and 25.9 mag arcsec^{-2} in *g*, *r*, and *i*, respectively.

2.3. Radio Continuum

We observed this system with the Karl G. Jansky Very Large Array (VLA) in the A configuration on 2015 August 20 using the *C*-band receiver, tuned to 4–6 GHz (λ = 7.5–5.0 cm). The on-source time is 42 minutes; we observed 3C147 for flux and bandpass calibrations, and we also observed J0920+4441 for phase calibration. Data reduction was carried out with CASA (McMullin et al. 2007) using the following steps: (i) standard calibration using the VLA Data Reduction Pipeline (C. Chandler et al. 2017, in preparation); (ii) removal of any portions of the data that were corrupted by strong radio frequency interference; and (iii) imaging with the task CLEAN. The imaging parameters are as follows: MT-MFS deconvolver with nterms of 2, 0″06 pixel size, and Briggs weighting with robust parameter of 0.5. The final image has a 0″39 × 0″35 synthesized beam and rms noise of 7 μJy beam^{-1} at the central pointing.

The radio flux of this source is about 37 ± 13 μJy at 5 GHz. Assuming that this emission is synchrotron-dominated and following a power law of $S \propto \nu^\alpha$ with a spectral index of $\alpha = -0.7$, we derive the radio luminosity of Satsuki to be 2.2×10^{20} WHz^1 at 1.4 GHz. This luminosity implies a SFR of 0.12 $M_\odot$ yr^{-1} using the Bell (2003) radio SFR indicator, converted to the Salpeter IMF, which is a factor of 2.5 greater than the limit implied by the Hα emission at the location of the radio source (see Table 1). Therefore, it is likely that this radio point source is a faint AGN.

2.4. H I

This source was observed as part of the HI-MaNGA program at the Robert C. Byrd Green Bank Telescope (GBT), which is
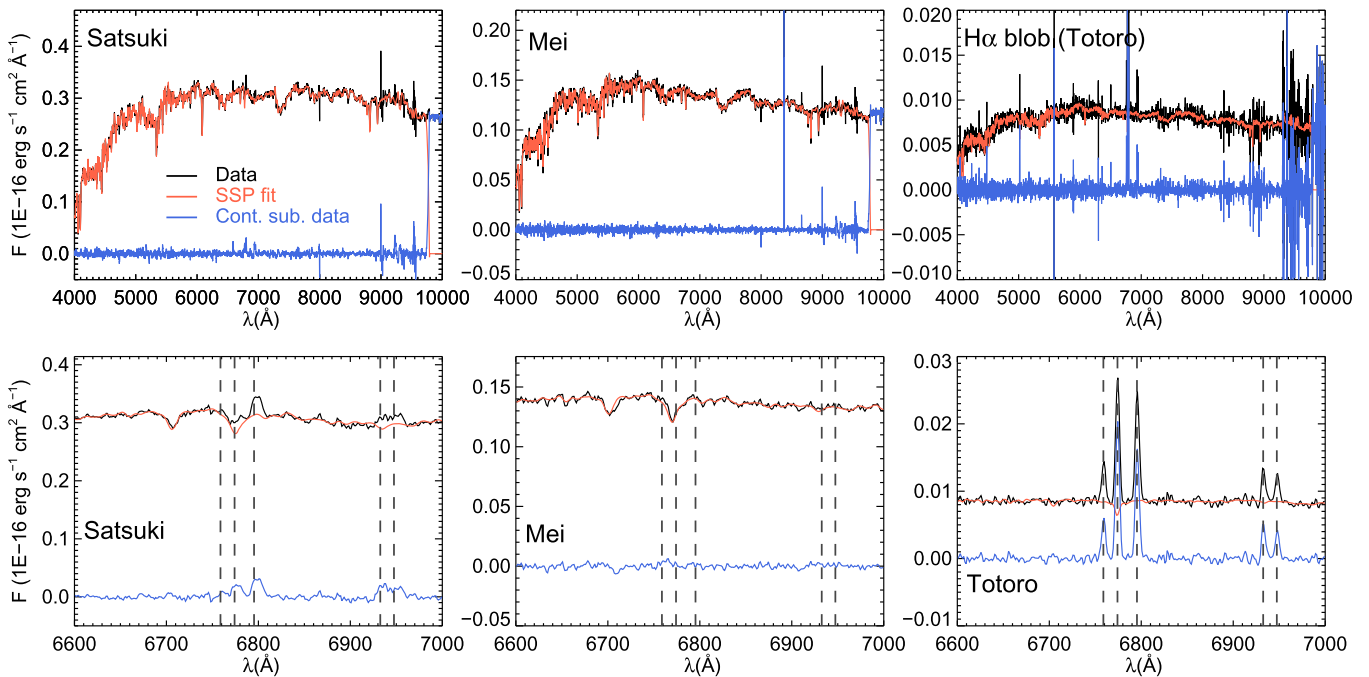
Figure 3. Upper panels: the black curves represent the MaNGA spectra of the central spaxel of the main galaxy "Satsuki" (left), the southern companion "Mei" (middle), and the Hα blob "Totoro" (right). The red curves are the best-fitted SSP model spectra for the stellar continuum. The blue curves show the residual spectra that are used for the emission line fitting. Lower panels: the zoom-in spectra around the Hα line. The five dashed lines denote the observed wavelengths of the [N II] 6584, Hα, [N II] 6584, [S II] 6717, and [S II] 6731 lines, respectively.

obtaining H I 21 cm observations of a large sample of MaNGA galaxies (AGBT16A_095, PI: K. Masters). This target was observed on 2016 February 5 for 3 sets of 5 minute ON/OFF pairs using the VEGAS spectrometer with a bandwidth of 23.44 MHz, centered on the frequency of 21 cm emission redshifted to cz = 9653 km s^{-1}. At this frequency the FWHM of the GBT beam is 9′. No H I emission was detected in this volume to a rms of 1.58 mJy (after smoothing to 5.15 km s^{-1} velocity resolution). Assuming a velocity spread of 100–400 km s^{-1}, this non-detection sets a 1σ upper limit of (8.9–9.2) ×10^8 $M_\odot$ for the H I mass of this system.[28]

2.5. X-Ray

Satsuki is located within the field of view of the ∼47 ks *Chandra* ACIS observation OBSID 4194 (PI: Trevor Ponman) that occurred on 2003 September 17. This pointing observation was centered on the nearby galaxy NGC 6338 (258.84256, +57.407) [J2000], ∼2' south of the MaNGA source of interest. Before the analysis, this data set was reprocessed using the Chandra_repro task in CIAO v4.8 (Fruscione et al. 2006) using CALDB v4.6.3.

The exposure-corrected image of this field (Figure 4) was generated using the "fluximage" command and the image indicates diffuse X-ray emission coincident with the dry merger system, as shown in Pandge et al. (2012), which performed a study on a nearby BCG based on the same X-ray data set. The spectrum of the X-ray emission coincident with the Hα blob of interest was then extracted using the CIAO script specextract using a source region of a 22″ × 18″ ellipse centered at 17:15:23.7, +57.26:05, which encompasses all of the emission.

We fit this X-ray spectrum with a single absorbed APEC model —the emission spectrum from a collisionally ionized diffuse gas—assuming the redshift of z = 0.032202 measured from the optical spectroscopy using XSPEC v12.8.2e (Arnaud 1996). This fit results in a reasonably reduced χ^2 (1.45 for 88 d.o.f), though it somewhat under-predicts the flux of >5 keV. As we will mention in Section 3.5, this dry merger system is part of a small group. The derived X-ray temperature is 1.26 ± 0.06 keV, consistent with the temperature on a group scale (Kettula et al. 2013). No point-like source is found within Satsuki or Totoro, indicating that there is no strong X-ray AGN present in this system.

3. Results

3.1. The Optical Morphology

To ensure that the absence of the optical counterpart at the position of Totoro as shown in Figure 1 is not due to a relatively shallow depth of SDSS imaging, we carried out a follow-up observation for this system with CFHT/MegaCam and combined it with the archival data (see Section 2.2). Figure 5 displays the *gri* composite image of this galaxy. It is clear that there are extended stellar halos surrounding the two galaxies. Again, at the position of the Hα blob, no apparent optical continuum is revealed (see the right panel of Figure 5).

To more clearly see the underlying surface brightness structure at the location of Totoro, we build detailed photometric models for the merging system using GALFIT v3.0.2 (Peng et al. 2002, 2010).The MecaCam *g*-band image is used for this purpose because it may better reveal the continuum of Totoro if it has had recent star formation (see Section 4). Since we are not interested in the overall structures of this complex merging system, we will only focus on a 400 × 400 pixel region centered on the MaNGA bundle. We construct a mask image to

---

[28] It is intended that HI-MaNGA data will be released as an SDSS Value Added Catalog in a future data release from SDSS. In addition, the raw data will be publicly available via the NRAO Data Archive at https://archive.nrao.edu a year following the observations.

Table 1
Properties of MaNGA 1-24145 (Satsuki), Its Southern Companion (Mei), and the Hα Blob (Totoro)

Object	z	R.A.	Decl.	M_* ($M_\odot$)	$M_{\rm H\,II}$ ($M_\odot$)	$M_{\rm H2}$ ($M_\odot$)	$M_{\rm H\,I}$ ($M_\odot$)	$M_{\rm halo}$ ($M_\odot$)	SFR (yr^{-1} $M_\odot$)
Satsuki	0.0322	258.84695	57.43288	1.2×10^{11}	⋯	⋯	$<9.2 \times 10^{8}$	⋯	<0.049[b]
Mei	0.0322	258.84750	57.43133	4.0×10^{10}[a]	⋯	⋯	$<9.2 \times 10^{8}$	⋯	⋯
Totoro	0.0322	258.84314	57.43529	⋯	8.2×10^{4}	$<1.2 \times 10^{8}$	$<9.2 \times 10^{8}$	5.6×10^{9}	<0.059[b]

Notes.
[a] This is scaled from the stellar mass of Satsuki by using the difference in their SDSS r-band magnitudes.
[b] This upper limit is derived assuming all the Hα fluxes come from the star formation.
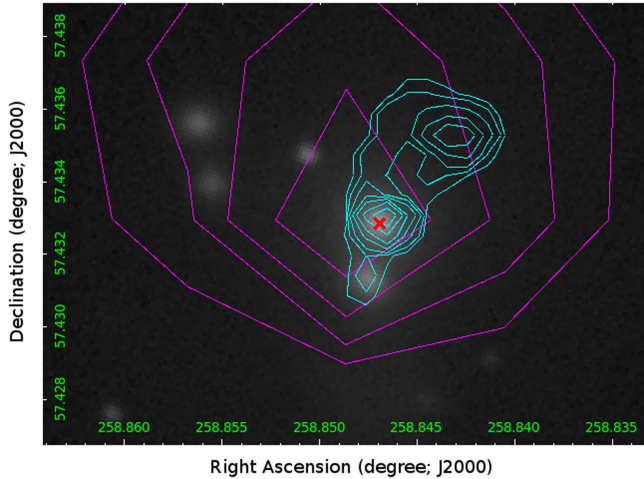
Figure 4. *Chandra* X-ray contours (magenta) and extinction-corrected MaNGA Hα contours (cyan) overlaid on the SDSS r-band image (background image) of MaNGA 1-24145. The red cross marks the position of the VLA point-source detection. The X-ray contours correspond to 44%, 30%, 21%, and 15% of the peak value, respectively, whereas the Hα contours correspond to 100%, 60%, 37%, 23%, 14%, 8%, 5%, 3%, and 2% of the peak value, respectively.

exclude isolated objects around the merging system from the fitting. The PSF of the image was modeled using the `SExtractor` and `PSFex` routines, and the PSF image used in the modeling was extracted using the central coordinate of the MaNGA bundle. Meanwhile, on top of the extended envelope, there are 11 objects (most are galaxies) that cannot be easily masked out. We model them separately, then subtract them from the image. All of these smaller objects can be modeled by a single- or double-Sérsic model locally with the help of an additional Sérsic and sky component to account for the envelope in the background. As shown in the panel (B) of Figure 6, these small objects have been removed smoothly from the input image without a significant residual pattern. Using this "cleaned" image as an input, we model the two merging galaxies along with their "common envelope" together using different combinations of Sérsic components. We started with three Sérsic components (one for each galaxy, and an additional one for the envelope), and gradually build up the complexity by adding more Sérsic components. As we simply want to achieve a smooth residual map to study the underlying structure, the number of Sérsic components and the detailed parameters are not a concern as long as each component behaves normally (e.g., Gu et al. 2013). For each object (including the envelope), all Sérsic components are constrained to have the same center, and only symmetric Sérsic components are used here. After visualizing the residual of the initial model, it becomes clear that, on the lower part of the image, there is an additional surface

brightness enhancement (caused by the merging process) that is not well fit by the simple model. Eventually, the best model we achieved included seven Sérsic components, plus a tilted-plane sky background component. Both of the merging galaxies, and the extended envelope, are described by two Sérsic components, while the surface brightness in the south is modeled using a single Sérsic component. All of the components behave regularly in terms of their size and shape, and except for the central component of the brighter galaxy, no component has a Sérsic index larger than 2.0.

Panels (C) and (D) of Figure 6 show the model image and the residual maps of this model reconstruction, respectively. It clearly reveals a rich system of shells and tidal tails around the main MaNGA galaxy, indicating an ongoing interaction between these two galaxies. Although the residual map is not perfectly smooth, no optical counterpart is found at the position of Totoro.

Reducing the number of components used or changing the initial parameters will not affect the above conclusion. The addition of more components could not further improve the residual map, but rather, could result in ill-behaved Sérsic components. Given the complex nature of this merging system, we also try to invoke the asymmetric features in `GALFIT`, especially in the 1st (global lopsidedness) and 4th (boxiness of the isophote) Fourier components (see Peng et al. 2010 for details). The residual map shows improvements around the tidal features, but does not change the conclusion that there is no apparent optical counterpart for Totoro.[29]

3.2. Kinematics from the MaNGA Observations

Figure 7 displays the velocity and dispersion maps for this system. While the stellar velocity field indicates that the main galaxy Satsuki is primarily pressure supported, the gas component reveals more complex structures. The central galaxy shows a weak rotation structure, while there is a strong variation in the line of sight velocity across the Totoro region, redshifted in the left tail and blueshifted in the right tail. The inconsistent velocity fields between stars and gas suggest that some part of the gas of Satsuki might have been either accreted or ejected recently. In the former case, it is similar to the ETGs, which exhibit misaligned gas and stellar kinematics, the so-called early-type "counter rotators" (Sarzi et al. 2006; Davis et al. 2011; Chen et al. 2016; Jin et al. 2016), although, the counter rotators in general are defined for systems with a rotating stellar component. The gas inflow scenario is also consistent with the Hα morphology, which shows bridge (tail)-like structures that connect Totoro and Satsuki. On the other hand, the complicated velocity field can also be explained if the

---

[29] The results still hold if we repeat the analysis using the i-band image, which is more sensitive to the stellar mass distributions.
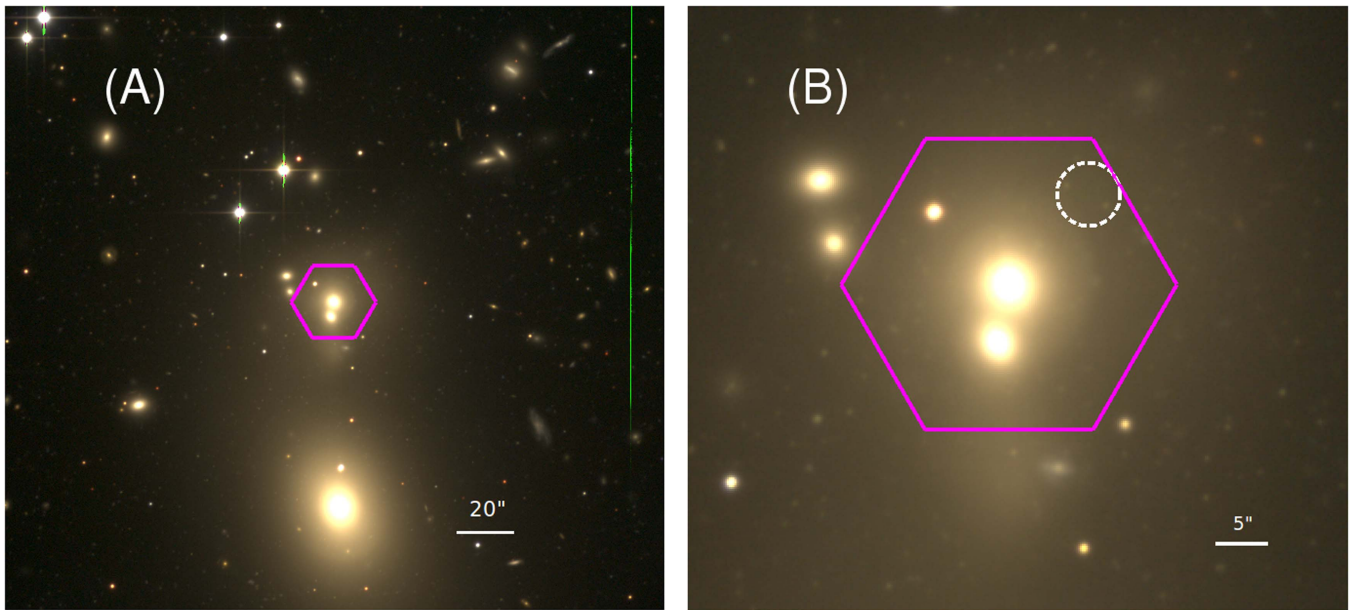
Figure 5. (A) CFHT *gri* composite color image for MaNGA 1-24145 with the MaNGA hexagonal FoV overlaid. A bright BCG is ∼43 kpc away to the south. (B) A zoomed-in picture of (A). The white circle marks the location of Totoro. In both panels, north is up and east is left.
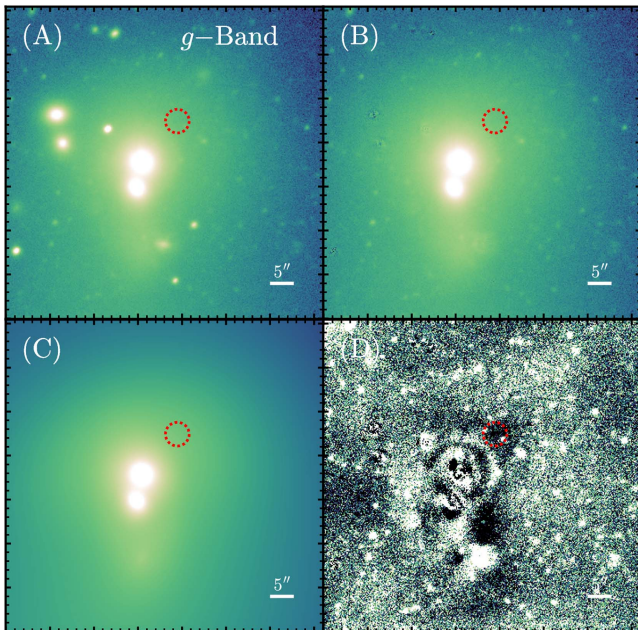
Figure 6. (A) The original CFHT Megacam *g*-band image, (B) the *g*-band image after subtracting nearby satellite galaxies, (C) a model image for (B), and (D) the residual images produced by GALFIT. The dashed white circles mark the position of Totoro. The white bars in the lower-right corner of each panel correspond to a scale of $5''$.

main galaxy Satsuki underwent a strong outburst phase, during which Totoro was expelled from Satuski.

3.3. Excitation State

In addition to the Hα and two [N II] 6584 lines, some other weak lines such as [S II] 6717,6731 and [O III] 5007 are also detected in both Satsuki and Totoro, allowing us to probe the ionization state for this system. Figure 8 shows the [O III] 5007/Hβ ratio, one of the frequently used ionization parameters, as a function of the distance from the main galaxy.

There exists a strong [O III] 5007/Hβ gradient, decreasing from the main galaxy Satsuki (location A) to the left bridge (locations B, C, and D) that connects to Totoro (location E, F, G, H, and I). On the other hand, the [O III] 5007/Hβ ratio is nearly constant across Totoro.

The multiple line detections also allow us to classify the emission line regions into H II or AGN regimes using the standard Baldwin–Phillips–Terlevich (BPT; Baldwin et al. 1981; Veilleux & Osterbrock 1987; Kauffmann et al. 2003; Kewley et al. 2006) excitation diagnostic diagrams. Here we apply three types of line diagnostics based on four line ratios, [O III] 5007/Hβ, [N II] 6584/Hα, [S II] 6717,6731/Hα, and [O I] 6300/Hα. Figures 9 and 10 display the line ratio diagrams and classification maps for this system, respectively. We adopt the dividing curves suggested in the literature (e.g., Kewley et al. 2001; Kauffmann et al. 2003; Cid Fernandes et al. 2010) to separate various regions. All three of the classifications indicate "LINER"-type excitations for Satsuki. As the LINER emission is extended across the entire main galaxy, this object falls into the extended LIER (eLIER) category, according to the classification scheme by Belfiore et al. (2016a, 2016b).

On the other hand, in the regions of Totoro, the line ratios are consistent with the "composite," "H I," and "LINER" regions when using the [N II], [S II], and [O I] diagnostics, respectively. In the remaining part of this paper, we treat Totoro as "composite" regions based on the [N II], as it allows for the intermediate excitation state as opposed to the other two methods.

3.4. Gas Metallicity

To further understand the properties of Totoro, we also measure the gas-phase metallicity (*Z*) for this system. Conventionally, there are many ways to estimate the gas metallicity through emission line ratios (see Kewley & Ellison 2008). However, most of those tracers are calibrated against the H II regions, and may not be applicable to systems with ionization parameters or interstellar medium pressure
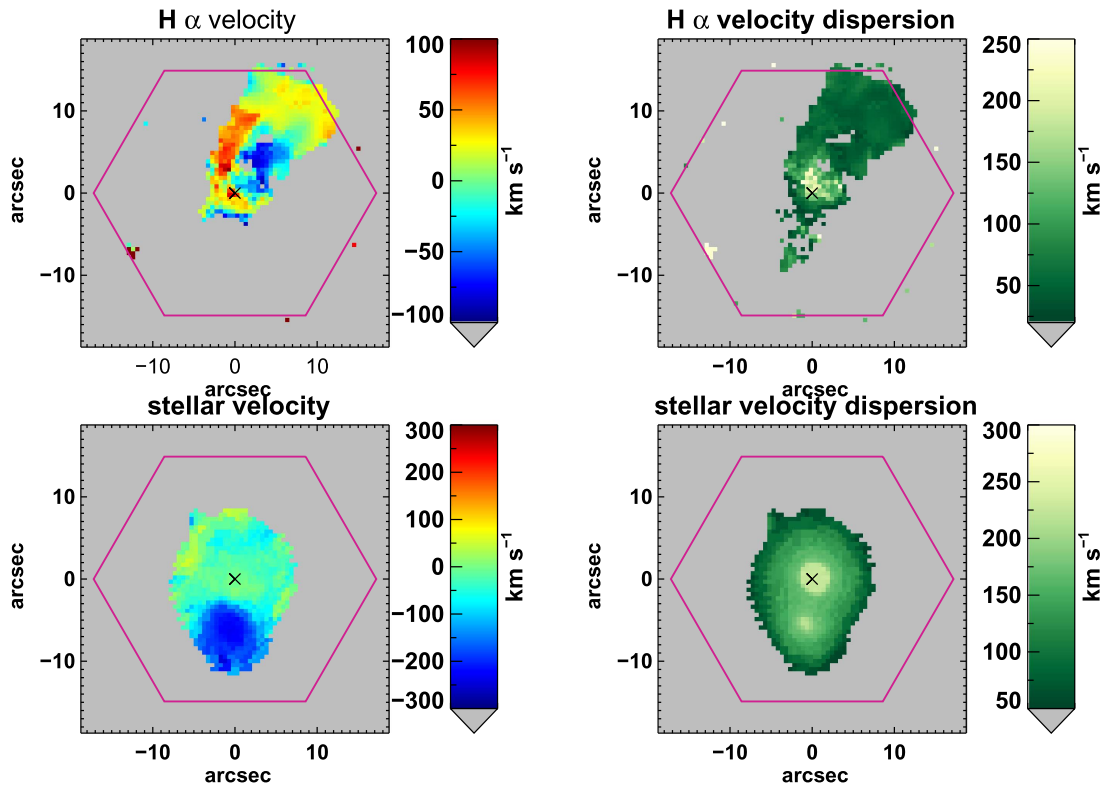
Figure 7. Velocity fields of MaNGA 1-24145 based on Hα line (upper panels) and stellar components (lower panels). The left panels show the radial velocities and the right panels show the velocity dispersions.

different from typical H II regions. Here, we adopt the "N2S2Hα" calibrator, which is suggested to be less sensitive to the ionization parameters (Dopita et al. 2016), to estimate the metallicity. The N2S2Hα calibration can be expressed as the following,

$$12 + \log (O/H) = 8.77 + N2S2H\alpha, \qquad (1)$$

where N2S2Hα = Log([N II]/[S II]) + 0.264Log([N II]/Hα). The [N II]–[S II] ratio is found to be nearly independent of the AGN luminosity and hence is a good metallicity indicator for even AGNs (Stern & Laor 2013). However, we note with caution that the derived metallicity may still be subject to large systematic uncertainty since the line ratios of the main galaxy and Totoro are located in the LINER and composite regions, respectively.

Figure 11 shows the Z(N2S2Hα) map for this system. The metallicity of the gas around Satsuki is close to solar and is ~0.3 dex lower than the expected value (Z = 9.1) for a massive galaxy with a stellar mass of $10^{11} M_\odot$, based on the local mass–metallicity relation (Tremonti et al. 2004). The offset we see here, however, may be easily accounted for by the different metallicity calibrators adopted. On the other hand, the averaged metallicity in the Hα region is greater for Totoro than Satsuki by a factor of 0.3 dex and is more consistent with the gas metalltcity of high-mass galaxies. Although the difference is significantly larger than the statistical uncertainty (0.03 dex–0.1 dex) in the metallicity measurement, it is difficult to interpret this result given the systematic uncertainty in the metallicity measurement due to their different ionization states.

3.5. Environment

The environment of this system is rather complex. As already mentioned, it has an early-type companion (Mei) just 4 kpc away to the south, which makes it a possible dry merger candidate. Moreover, Satsuki is also part of the system MCG +10+24–117, a small group falling onto a galaxy cluster with NGC 6338 as a central Brightest Cluster Galaxy that is 43 kpc away to the south (see Figure 5; Pandge et al. 2012; Dupke & Martins 2013).

4. Discussion

4.1. The Origin of the Hα Blob

Using the first-year MaNGA data, we discover a giant Hα blob, Totoro, associated with a dry merger system. This object, however, does not have any optical counterparts down to 26.9 mag arcsec^{-2} in deep CFHT/MegaCam g, r, and i images. There are several possible scenarios to explain the origins of Totoro.

Scenario 1: Totoro is associated with gas tidally stripped from Satsuki during the interaction between Satsuki and Mei.

Scenario 2: Totoro is associated with the gas ram-pressure stripped during the infall of Satsuki toward the center of NGC 6338 galaxy cluster, similar to the NGC 4569 located in the Virgo cluster (Boselli et al. 2016).

Scenario 3: Totoro is associated with gas ejected from Satsuki by an AGN outflow during the merger between Satsuki and Mei. If the central black hole of Satsuki is turned on during mergers, the energy can ionize the stripped gas, resulting in Hα emissions, similar to the known "Hanny's Voorwerp" phenomenon (Lintott et al. 2009).
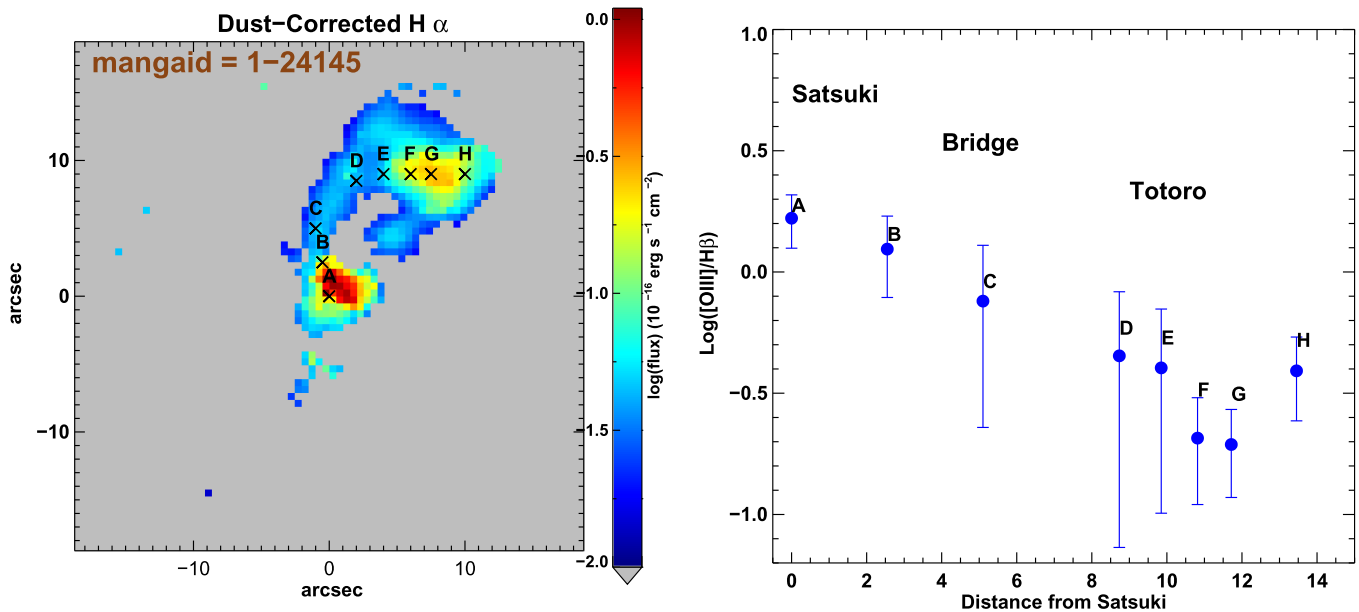
Figure 8. Left: the extinction-corrected Hα map of MaNGA 1-24145. Right: the [O III] 5007/Hβ ratio as a function of distance from the center of Satsuki. The letters (A, B, C, etc.) mark the different locations of this system.

Scenario 4: Totoro is a UDG (or alternatively, an LSB galaxy), which falls below the detection limit (26.9 mag arcsec^{-2} in r-band) of CFHT imaging data, making it a "dark" galaxy. The morphology of Totoro (Figure 1), especially the (tail) bridge-like structures that connect between Satsuki and Totoro, indicate that Satsuki is likely under the interaction with the hosting galaxy of Totoro, which has a comparable physical size as Satsuki.

To estimate the mass of the warm gas component, we follow the approach adopted by Cheung et al. (2016b). We first estimate the electron density n_e to be ~260 cm^{-3} based on the median value of the [S II]6717–[S II]6731 ratio in the region of Totoro following Equation (3) of Proxauf et al. (2014), which assumes an electron temperature of $T_e = 10,000 K$. Next, we calculate the extinction-corrected Hβ luminosity, $L_{H\beta}$, to be 3.1×10^{39} erg s^{-1}. The ionized gas mass can then be derived using the following equation (Osterbrock & Ferland 2006; Fu et al. 2012):

$$\frac{M_{H\,II}}{6.8 \times 10^7 \, M_\odot} = \left(\frac{L_{H\beta}}{10^{40} \text{ erg s}^{-1}}\right)\left(\frac{n_e}{1 \text{ cm}^{-3}}\right)^{-1}. \quad (2)$$

We obtain the ionized gas mass ~$8.2 \times 10^4 \, M_\odot$.

The H I observation of this system provides an upper limit of $(8.9–9.2) \times 10^8 \, M_\odot$ for the H I mass due to the null detection. We account for the He gas by applying a factor of 1.33 to the upper limit. We can also infer the H$_2$ content of this Totoro using the Hα emission. The integrated Hα flux over the spaxels within the Totoro region is 3.3×10^{-15} erg s^{-1} cm^{-2}, corresponding to a luminosity of 7.8×10^{39} erg s^{-1}. Assuming all of the Hα flux results from star formation, we obtain the total SFR of Totoro to be 0.059 $M_\odot$ yr^{-1} using the conversion between the Hα luminosity and the SFR from Kennicutt (1998). We then estimate the total H$_2$ gas mass (= SFR × t_{dep}) of the Hα blob to be ~$1.2 \times 10^8 \, M_\odot$, assuming a typical gas depletion time (t_{dep}) of 2 Gyr. This value is also an upper limit since we have assumed that all of the Hα fluxes are contributed by the star formation. This implies an upper limit of the entire cold gas (H I + He + H$_2$) of ~$1.3 \times 10^9 \, M_\odot$.

Although Satsuki and its companion Mei are consistent with being ETGs, the amount of cold gas in Totoro is not unexpected if it is part of Satsuki. For example, recent works have found that a significant fraction of massive ETGs that show signs of star formation possess cold gas with a gas mass comparable to Totoro (O'Sullivan et al. 2015; Davis et al. 2016). Therefore, it is reasonable to speculate that Totoro may originally be part (if not all) of the cold gas contained in Satsuki, and then the cold gas is ejected during the galaxy–galaxy interaction or it is ejected because of the ram-pressure stripping (scenarios 1–3, respectively).

To test the galaxy interaction scenario (scenario 1), we performed and examined a set of N-body simulations of the interaction of two Elliptical galaxies (E–E) with the code Gadget2 (Springel 2005). Different initial orbital configurations (e.g., pericentric distance) have been considered following the methods of Peirani et al. (2010). Although we did not include a gas component in our dry merger simulations, the features of the stellar components can still be useful to understand the system, as the stellar streams trace the gas streams before 1 Gyr during galaxy interaction.

Among all the cases we have looked at, we did not see the formation of any clear stellar stream or a centrally concentrated blob-like structure during the interaction. This strongly suggested that Totoro is unlikely to be produced during an E–E interaction. In addition, based on other existing gas-rich merger simulations (see, for instance, Barnes & Hernquist 1996; Di Matteo et al. 2007; Peirani et al. 2010), the prominent gas (or stellar) streams are expected to be formed when at least one of the merger progenitors has extended disk structures. This is unlikely to be the case for this dry merger system, even if these two ellipticals have small amount of gas. Furthermore, the latter simulations also suggest that it is very difficult to produce such a blob-like structure. Although tidal dwarf galaxies can be formed during the interaction of disk galaxies (see, for instance, Bournaud et al. 2003; Duc et al. 2004) in these cases, the blob-like structure is more extended without clear star formation activity. Nevertheless, we note that the
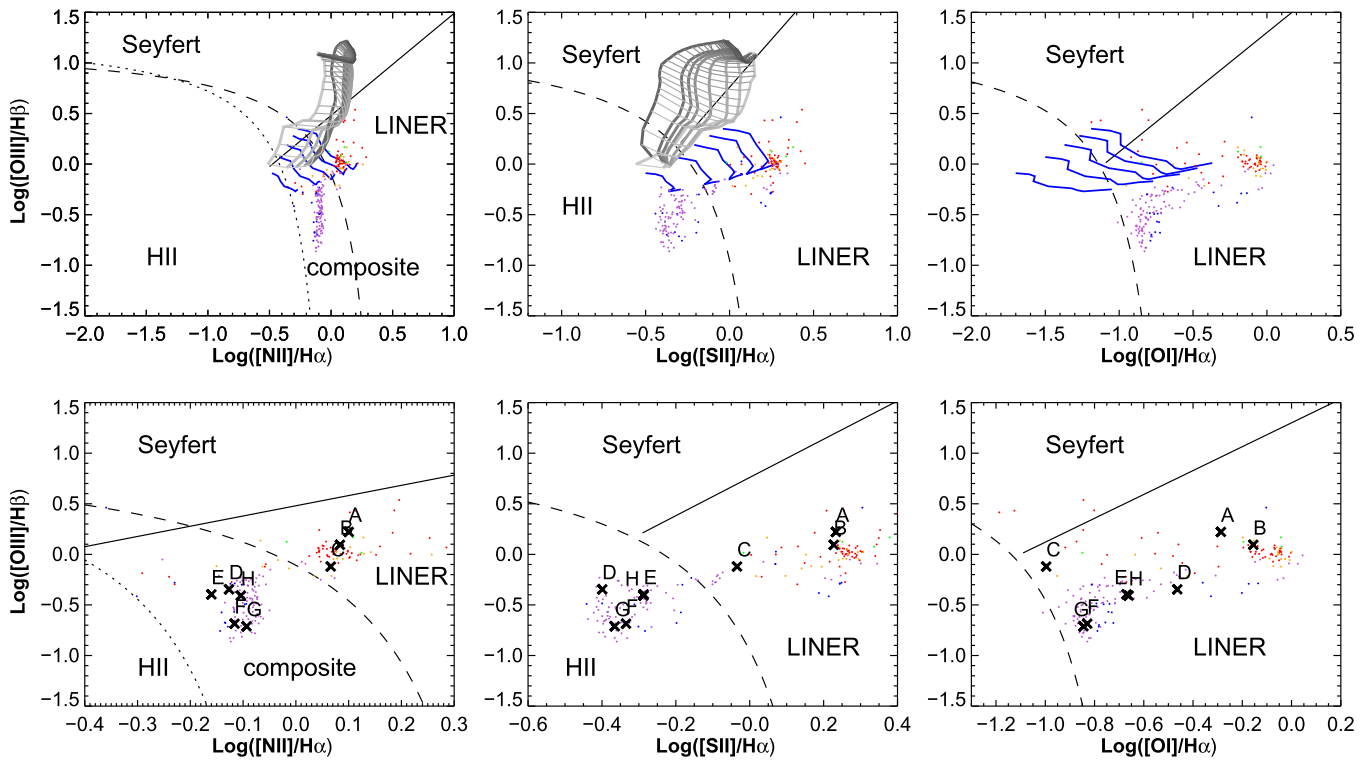
Figure 9. Upper panels: BPT diagnostic diagrams for MaNGA 1-24145 based on the [O III] 5007/Hβ vs. [N II] 6584/Hα (left panels), [O III] 5007/Hβ vs. [S II] 6717,6731/Hα (middle panels), and [O III] 5007/Hβ vs. [O I] 6300/Hα (right panels). Various colors on the data points indicate the physical separation from the center of Satsuki (from near to far: red, origin, green, blue, purple). The solid, dashed, and dotted lines show the classification lines suggested by Cid Fernandes et al. (2010), Kewley et al. (2001), and Kauffmann et al. (2003), respectively. The blue curves display the model predictions of the shock and photoionization mixing sequences by Ho et al. (2014). Each line corresponds to a certain shock fraction (from bottom to top: 20% to 100%). The shock velocity ranges from 100 to 300 km s^{-1} (from left to right). The MAPPINGS III shock+precursor models (gray grid) with $n = 1$ cm^{-3} from Allen et al. (2008) are also shown for comparison. The thick lines represent the constant magnetic parameter while the thin lines display the constant shock velocity ranging from 200 to 1000 km s^{-1} (bottom to top; with 25 km s^{-1} intervals). Bottom panels: a zoomed-in view of the upper panels. The letters (A, B, C, etc.) mark the different locations of this system, following the definitions of Figure 8.

simulations we have examined have the following caveats: (i) the parameter space is too large to be fully explored, and (ii) the stellar/AGN feedback that could drive galactic scale outflows and these physics are not included. Such advanced simulations are beyond the scope of this work. We defer more detailed comparisons with simulations to a future work.

On the other hand, the centrally concentrated blob-like structure is not expected in the ram-pressure stripped gas (scenario 2) either, which often shows tail- and/or "jellyfish"-like structures (e.g., Boselli et al. 2016). Moreover, galaxies that show ram-pressure stripping phenomena are mostly gas-rich late-type galaxies, unlike Satsuki.

Another explanation for Totoro is it being the materials ejected by an AGN located in Satsuki (scenario 3), similar to the extended emission-line regions found around the quasars (Fu & Stockton 2007a, 2007b). The outflow scenario is also consistent with the complicated velocity field that is seen in the gas component of this system. As discussed in Section 2, we do not detect an X-ray point source or an extended radio jet in the main galaxy, suggesting that there is no strong ongoing AGN activity. However, it has been known that the AGN brightness can vary over timescales of several to 10^5 years (Denney et al. 2014; LaMassa et al. 2015; McElroy et al. 2016), either due to a change in the black hole accretion rate or tidal-disruption events (e.g., Saxton et al. 2012; Merloni et al. 2015). Therefore, we cannot rule out the possibility of a recent past AGN outflow, similar to the notable phenomena of Henny's Voorwerp, in which a clump of ionized gas is found several

kpc away from a galaxy while the ionizing source has already diminished. Nevertheless, it is still unclear why the ejected gas would have a higher metallicity than that of the gas remaining in Satsuki (although it is unclear whether the metallicity difference is real, given the potential systematics in our metallicity estimate).

An alternative explanation of the Hα blob is a separate faint galaxy, interacting with the dry merger system (scenario 4). A few morphological features such as, for example, the centrally concentrated Hα and the bridges extended from Totoro toward Satsuki, are the most consistent with Totoro being a separated gas component. According to numerical simulations, these features can be explained by the interaction between the main galaxy and a faint disk galaxy (scenario 1) (see, for instance, Peirani et al. 2010; Cheung et al. 2016a).

Recently, a class of UDGs was identified in the Coma cluster and several low-redshift clusters (van Dokkum et al. 2015; Davies et al. 2016; van der Burg et al. 2016). These UDGs are surprisingly large in size ($r_{\rm eff} = 1.5$–4.6 kpc), despite their low stellar masses ($<10^8$ $M_\odot$). The majority of these UDGs are found to lie on the red-sequence, indicating old stellar populations and quenched star formation activities (van der Burg et al. 2016). Possible formation mechanisms include gas being stripped by the ram pressure when falling into the cluster, which prevents the subsequent star formation, or gas being expelled due to the strong stellar or supernova feedback for galaxies with a halo mass between 10^{10} and 10^{11} $M_\odot$ (Di Cintio et al. 2017). Nevertheless, it remains an open question
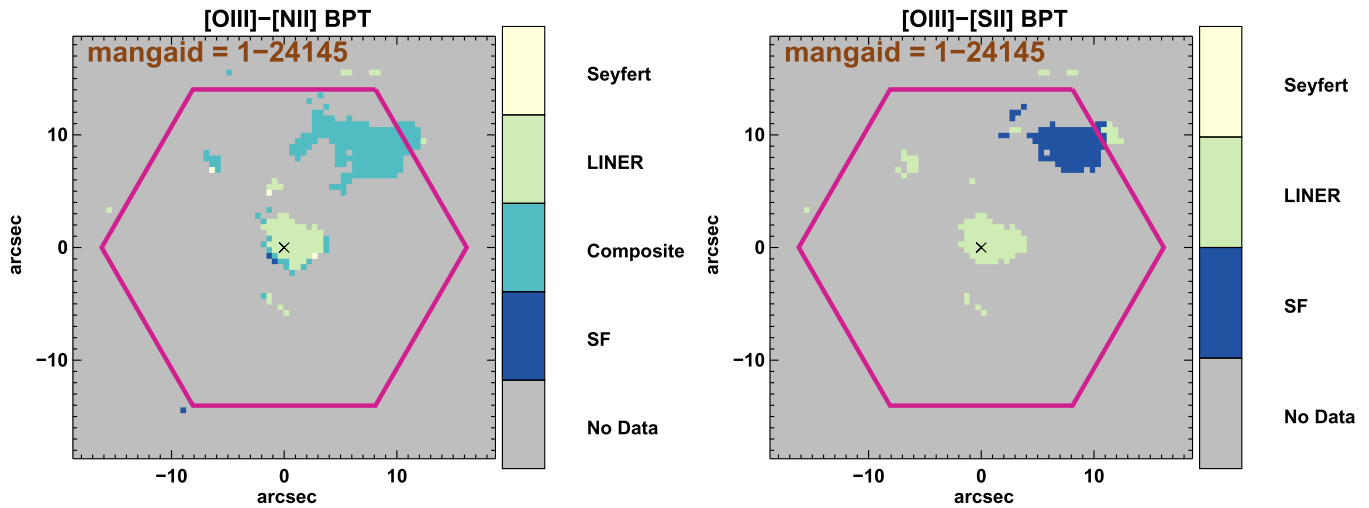
Figure 10. BPT classification maps for MaNGA 1-24145 based on the [O III] 5007/Hβ vs. [N II] 6584/Hα (left panel) and [O III] 5007/Hβ and [S II] 6717,6731/ Hα (right panel). The [O I] diagnostic map is not included here as all spaxels are classified as LINER.
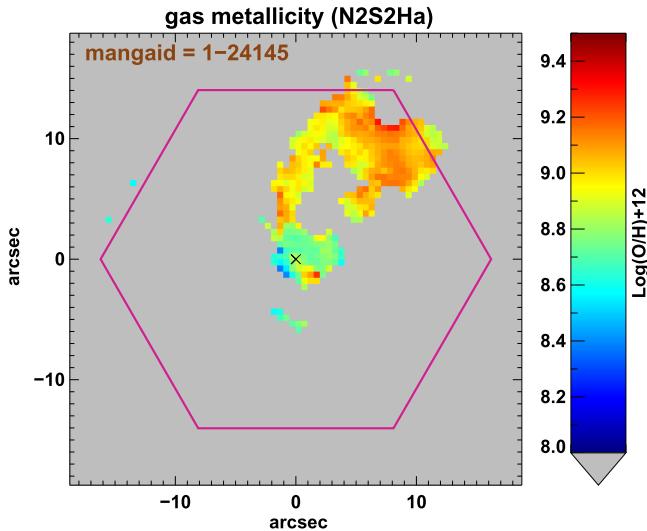
Figure 11. The gas metallcity map of MaNGA 1-24145, computed using the method described in Dopita et al. (2016), based on the emission line ratios among [N II], [S II], and Hα.

regarding the origin of UDGs and whether these UDGs are already quenched before falling into the cluster environments. Totoro identified in this work has a comparable size ($\sim$3.2 kpc) to the UDGs. However, the averaged surface brightness of Totoro has an upper limit of 26.9 mag arcsec^2, at least 1–3 mag dimmer compared to that of the known UDGS ranging from 24 to 26 mag arcsec^{-2}. Another aspect of Totoro that is distinct from the known UDGs is that the latter are generally old in the stellar populations, as indicated from their red colors, whereas Totoro is likely to have small amount of ongoing star formation based on the BPT diagnostics but with fewer old stellar populations. Therefore, Totoro may represent a different category of LSB galaxies from the quiescent UDGs.

The nondetection of optical light associated with Totoro can provide an upper limit for the amount of star formation. Assuming that this Hα cloud is a young star-forming system with an age of <0.1 Gyr, the flux in the optical regime is expected to be comparable to that in the UV (1500–2800 Å) in the case of no dust extinction. Following the conversion between the UV luminosity, Hα luminosity, and the SFR given

by (Kennicutt 1998) and adopting the surface brightness limit (26.9 mag arcsec^{-2}) from our CFHT MegaCam r-band observation, we estimate that the corresponding Hα surface density of this Totoro is on the order of 1.1×10^{-17} erg s^{-1} cm^{-1} arcsec^{-2}, which is one magnitude lower than the peak value of Totoro. By integrating it over the Hα region, we estimate that the star formation contributes to less than 37% of the total Hα flux, or otherwise we should be able to detect the optical counterpart.

Given the very low amount of star formation that can possibly occur in Totoro, we speculate that Totoro is a gas cloud that fails to form stars efficiently, and thus is a "dark" gas cloud. The origin of this gas cloud, whether it is associated with a satellite dark matter or a pure gas cloud, is difficult to pin down. However, the latter scenario is unlikely since it would be difficult to maintain the kiloparsec-scale gas cloud against gravity without invoking the existence of a dark matter halo. If Totoro is indeed hosted by a subhalo, it would be a strong evidence of the existence of "dark" subhalos, which help to alleviate the missing satellite problem. Since there is no stellar component in the region of Totoro, we could roughly estimate the halo mass of Totoro based on the gas velocity dispersion using the viral theorem. Taking $R = 3.2$ kpc and $\sigma_{gas} = 50$ km s^{-1}, we obtain the halo mass $M_{halo} \sim 5.6 \times 10^9 \, M_\odot$.

The high metallicity of Totoro (see Section 3.4) is unexpected for a typical dwarf galaxy. One possible explanation for this is that the gas cloud has been enriched by the surrounding environment, and may have a different evolution process from other typically known dwarf galaxies. However, we caution that the metallicity measurement presented in this work is subject to large uncertainty since the ionization source is not well constrained.

4.2. Sources of Ionization

Shocks can often lead to line ratios similar to those occupying the composite regions (Ho et al. 2014). In the case where there are shocks, the gas velocity dispersion (σ_{gas}) is expected to be as high as several hundreds of km s^{-1}. As revealed in Figure 7, σ_{gas} in the region of Totoro is $\sim$50 km s^{-1}. Although it is close to the lower end of the velocity dispersion

distribution that has been found in typical shocked regions, we cannot rule out the shock excitation of the emission lines. To gain insight into whether the shock is responsible for producing the ionized ratios in this system, we show the shock and photoionization mixing models from Ho et al. (2014) as blue curves in the upper panels of Figure 9. These models are produced based on the `MAPPINGS IV code` (Dopita et al. 2013) and span a wide range of shock fractions (from 20% to 100%) and shock velocities (from 100 to 300 km s^{-1}). As noted, the models predict a greater [O III] 5007/Hβ ratio than what is observed in the data and do not cover the majority of the regions occupied by the data points even at a shock velocity up to $\sim$300 km s^{-1}. In addition to the pure shock models, we also compare the data to the shock + precursor models of Allen et al. (2008) with $n = 1$ cm^{-3} and solar metallicity shown as the gray grid in Figure 9. Although the grid starts with the shock velocity of 200 km s^{-1}, it is expected by extrapolation that models with lower velocity values still cannot reproduce the [N II]/Hα ratios of Totoro. These comparisons suggest that shocks are unlikely to be the dominant mechanism that is responsible for ionization of the gas blob.

There have been studies showing that AGNs are able to ionize gas clouds extending to several kiloparsecs (Fu & Stockton 2008; Lintott et al. 2009), and the effect from AGNs may persist even $\sim$10^5 year after the central engines shut off (e.g., the "Hanny's Voorewerp"; Lintott et al. 2009). If Totoro is indeed a "dark" galaxy or a cloud interacting with Satsuki, the tidal field would cause a gas inflow that fuels the central black hole of Satsuki and possibly trigger the AGN activity. Although no X-ray point source is detected in the position of either Satsuki or Totoro, the detection of a point-like radio source (see Section 2.3) in the center of Satsuki indicates the presence of a low-activity AGN. Therefore, an alternative explanation for the line ratios seen in Totoro is due to the star formation–AGN mixing effect (Davies et al. 2014a, 2014b).

Observationally a starburst–AGN mixing sequence is often found in a starbursting galaxy that hosts a central AGN, in which case the line ratio moves from Seyfert, to composite, to H II regions as the distance from the central AGN increases. The position of line ratios depends on the fractional contribution between the AGN and star formation. According to the mixing model by Davies et al. (2014a), when the star-forming cloud is photonionized by an AGN, the line ratios can fall into the "composite" region on BPT diagrams. In the case of 100% contribution from an AGN, the emission line ratio falls into the "AGN" region, instead of the "composite" region where Totoro lies. This implies that the emission line ratios seen in Totoro cannot be fully attributed to pure AGN photonionization, and some level of star formation may be required. Unlike the typical star formation—AGN mixing (Davies et al. 2014a, 2014b), our case is analogous to the star formation—LINER sequence, in which the LINER excitation is due to the low-activity AGN located in Satsuki.

4.3. Comparison to Similar Objects in the Literature

There are several similar systems reported in the literature that show offset ionized gas components, and hence it is intriguing to compare this Totoro with previous cases. For example, the famous Hanny's Voorewerp (Lintott et al. 2009) also exhibits a separate warm gas component that is offset from the main galaxy by several kiloparsecs. However, there are several different features between Hanny's Voorewerp and Totoro. First, the ionized gas of Hanny's Voorewerp has a much higher excitation state and the line ratios are consistent with Seyfert, as opposed to the "composite" region for Totoro. Moreover, the Hα morphology of Hanny's Voorewerp is lumpy and irregular, unlike a disk-like structure seen in our case. Another well-known example is an Hα emission line component (often referred to as the "cap") at a projected distance of 11 kpc northwest of M82 (Devine & Bally 1999; Lehnert et al. 1999; Stevens et al. 2003). The cap has a shell-like structure and may possibly be a bow shock formed by the starburst-driven superwind. In both cases, the nearby galaxy is a late-type star forming galaxy, different from Satsuki, which is an early-type galaxy. Totoro may thus represent a different category of offset ionized gas in nearby galaxies.

5. Conclusion

Here we report a discovery of a puzzling giant Hα blob, Totoro, identified from the first-year MaNGA data. The data disfavor the scenario that Totoro is a tidally stripped gas from MaNGA 1-24145 (Satsuki) interacting with the southern companion (Mei), or that Totoro is the ram-pressure stripped gas from when Satsuki falls into the center of the cluster where it is located. Despite there being no X-ray point source or radio jet detected in Satsuki, given its radio luminosity, we cannot rule out the possibility that Totoro is ejected from past AGN activities in Satsuki. On the other hand, the Hα morphology and the lack of stellar tidal streams suggest that Totoro could also be a separate "dark" galaxy (or an extremely LSB galaxy) interacting with Satsuki. The nondetection of the stellar continuum suggests that Totoro is different from known dwarf populations or UDGs: it is either completely "dark" or with a SFR that contributes to <37% of the Hα flux.

As for the source that powers the line excitation for Totoro, the "composite" line excitation can be explained either by a star-forming cloud being excited by a low-velocity shock or by the star formation—LINER mixing effect. The shock scenario, however, is less favored because of the low velocity dispersion observed in this Totoro region. The decrease in the [O III] 5007/Hβ ratio away from Satsuki indicates that the ionizing source is possibly located inside Satsuki. Thus, the star formation—LINER mixing effect seems to be the most probable ionizing mechanism. In this scenario, the hypothesis is that the ionizing source is the low-activity AGN residing in Satsuki, being triggered by the gas inflow that is induced during the interaction between Satsuki and the "dark" galaxy (or gas cloud). The AGN subsequently photoionizes the "dark" gas cloud, which then emits the Hα photons.

However, we have not considered the case where Totoro is tidally stripped from Satsuki while falling into the cluster center at the same time, which results in the non-typical tidally or ram-pressure stripped gas morphology of Totoro. More sophisticated modeling considering both the effects of tidal disrupting and the orbital motions of Satsuki relative to the cluster environments, as well as future resolved atomic and molecular gas observations, such as H I and CO, are required to further understand the origin of Totoro.

References

Abraham, R. G., & van Dokkum, P. G. 2014, PASP, 126, 55
Allen, M. G., Groves, B. A., Dopita, M. A., Sutherland, R. S., & Kewley, L. J. 2008, ApJS, 178, 20
Arnaud, K. A. 1996, adass V, 101, 17
Baldwin, J. A., Phillips, M. M., & Terlevich, R. 1981, PASP, 93, 5
Barnes, J. E., & Hernquist, L. 1996, ApJ, 471, 115
Belfiore, F., Maiolino, R., Maraston, C., et al. 2016a, MNRAS, 461, 3111
Belfiore, F., Maiolino, R., Maraston, C., et al. 2016b, arXiv:1609.01737
Bell, E. F. 2003, ApJ, 586, 794
Boselli, A., Cuillandre, J. C., Fossati, M., et al. 2016, A&A, 587, A68
Bournaud, F., Duc, P. A., & Masset, F. 2003, A&A, 411, L469
Bundy, K., Bershady, M. A., Law, D. R., et al. 2015, ApJ, 798, 7
Cannon, J. M., Martinkus, C. P., Leisman, L., et al. 2015, AJ, 149, 72
Chen, Y.-M., Shi, Y., Tremonti, C. A., et al. 2016, NatCo, 7, 13269
Cheung, E., Bundy, K., Cappellari, M., et al. 2016a, Natur, 533, 504
Cheung, E., Stark, D. V., Huang, S., et al. 2016b, ApJ, 832, 182
Cid Fernandes, R., Stasińska, G., Schlickmann, M. S., et al. 2010, MNRAS, 403, 1036
Davies, J. I., Davies, L. J. M., & Keenan, O. C. 2016, MNRAS, 456, 1607
Davies, R. L., Kewley, L. J., Ho, I.-T., & Dopita, M. A. 2014a, MNRAS, 444, 3961
Davies, R. L., Rich, J. A., Kewley, L. J., & Dopita, M. A. 2014b, MNRAS, 439, 3835
Davis, T. A., Alatalo, K., Sarzi, M., et al. 2011, MNRAS, 417, 882
Davis, T. A., Greene, J., Ma, C.-P., et al. 2016, MNRAS, 455, 214
Denney, K. D., De Rosa, G., Croxall, K., et al. 2014, ApJ, 796, 134
Devine, D., & Bally, J. 1999, ApJ, 510, 197
Di Cintio, A., Brook, C. B., Dutton, A. A., et al. 2017, MNRAS, 466, L1
Di Matteo, P., Combes, F., Melchior, A. L., & Semelin, B. 2007, A&A, 468, 61
Dopita, M. A., Kewley, L. J., Sutherland, R. S., & Nicholls, D. C. 2016, Ap&SS, 361, 61
Dopita, M. A., Sutherland, R. S., Nicholls, D. C., Kewley, L. J., & Vogt, F. P. A. 2013, ApJS, 208, 10
Drory, N., MacDonald, N., Bershady, M. A., et al. 2015, AJ, 149, 77
Duc, P.-A., Bournaud, F., & Masset, F. 2004, A&A, 427, 803
Dupke, R. A., & Martins, S. 2013, in AAS/High Energy Astrophysics Division, HEAD Meeting #13, id.116.07
Falcón-Barroso, J., Sánchez-Blázquez, P., Vazdekis, A., et al. 2011, A&A, 532, A95
Fischera, J., & Dopita, M. 2005, ApJ, 619, 340
Fruscione, A., McDowell, J. C., Allen, G. E., et al. 2006, Proc. SPIE, 6270, 62701V
Fu, H., & Stockton, A. 2007a, ApJL, 664, L75
Fu, H., & Stockton, A. 2007b, ApJ, 666, 794
Fu, H., & Stockton, A. 2008, ApJ, 677, 79
Fu, H., Yan, L., Myers, A. D., et al. 2012, ApJ, 745, 67
Giovanelli, R., Haynes, M. P., Kent, B. R., et al. 2005, AJ, 130, 2598
Gu, M., Ho, L. C., Peng, C. Y., & Huang, S. 2013, ApJ, 773, 34
Gunn, J. E., Siegmund, W. A., Mannery, E. J., et al. 2006, AJ, 131, 2332
Gwyn, S. D. J. 2008, PASP, 120, 212
Hamer, S. L., Edge, A. C., Swinbank, A. M., et al. 2012, MNRAS, 421, 3409
Haynes, M. P., Giovanelli, R., Martin, A. M., et al. 2011, AJ, 142, 170
Ho, I.-T., Kewley, L. J., Dopita, M. A., et al. 2014, MNRAS, 444, 3894
Husemann, B., Sánchez, S. F., Wisotzki, L., et al. 2010, A&A, 519, A115
Jin, Y., Chen, Y., Shi, Y., et al. 2016, MNRAS, 463, 913
Kauffmann, G., Heckman, T. M., Tremonti, C., et al. 2003, MNRAS, 346, 1055
Keel, W. C., Chojnowski, S. D., Bennert, V. N., et al. 2012, MNRAS, 420, 878
Kennicutt, R. C., Jr. 1998, ARA&A, 36, 189
Kettula, K., Finoguenov, A., Massey, R., et al. 2013, ApJ, 778, 74
Kewley, L. J., Dopita, M. A., Sutherland, R. S., Heisler, C. A., & Trevena, J. 2001, ApJ, 556, 121
Kewley, L. J., & Ellison, S. L. 2008, ApJ, 681, 1183
Kewley, L. J., Groves, B., Kauffmann, G., & Heckman, T. 2006, MNRAS, 372, 961
Klypin, A., Kravtsov, A. V., Valenzuela, O., & Prada, F. 1999, ApJ, 522, 82
LaMassa, S. M., Cales, S., Moran, E. C., et al. 2015, ApJ, 800, 144
Law, D. R., Cherinka, B., Yan, R., et al. 2016, arXiv:1607.08619
Lehnert, M. D., Heckman, T. M., & Weaver, K. A. 1999, ApJ, 523, 575
Lintott, C. J., Schawinski, K., Keel, W., et al. 2009, MNRAS, 399, 129
McElroy, R. E., Husemann, B., Croom, S. M., et al. 2016, A&A, 593, L8
McMullin, J. P., Waters, B., Schiebel, D., Young, W., & Golap, K. 2007, adass XVI, 376, 127
Merloni, A., Dwelly, T., Salvato, M., et al. 2015, MNRAS, 452, 69
Moore, B., Ghigna, S., Governato, F., et al. 1999, ApJL, 524, L19
Osterbrock, D. E., & Ferland, G. J. (ed.) 2006, Astrophysics of Gaseous Nebulae and Active Galactic Nuclei (2nd ed.; Sausalito, CA: Univ. Science Books)
O'Sullivan, E., Combes, F., Hamer, S., et al. 2015, A&A, 573, A111
Pandge, M. B., Vagshette, N. D., David, L. P., & Patil, M. K. 2012, MNRAS, 421, 808

Peirani, S., Crockett, R. M., Geen, S., et al. 2010, MNRAS, 405, 2327
Peng, C. Y., Ho, L. C., Impey, C. D., & Rix, H. W. 2002, AJ, 124, 266
Peng, C. Y., Ho, L. C., Impey, C. D., & Rix, H.-W. 2010, AJ, 139, 2097
Proxauf, B., Öttl, S., & Kimeswenger, S. 2014, A&A, 561, A10
Sánchez, S. F., Pérez, E., Sánchez-Blázquez, P., et al. 2016a, RMxAA, 52, 21
Sánchez, S. F., Pérez, E., Sánchez-Blázquez, P., et al. 2016b, RMxAA, 52, 171
Sánchez-Blázquez, P., Peletier, R. F., Jiménez-Vicente, J., et al. 2006, MNRAS, 371, 703
Sarzi, M., Falcón-Barroso, J., Davies, R. L., et al. 2006, MNRAS, 366, 1151
Saxton, R. D., Read, A. M., Esquej, P., et al. 2012, A&A, 541, A106
SDSS Collaboration, Albareti, F. D., Allende Prieto, C., et al. 2016, arXiv:1608.02013
Smee, S. A., Gunn, J. E., Uomoto, A., et al. 2013, AJ, 146, 32
Springel, V. 2005, MNRAS, 364, 1105

Stern, J., & Laor, A. 2013, MNRAS, 431, 836
Stevens, I. R., Read, A. M., & Bravo-Guerrero, J. 2003, MNRAS, 343, L47
Tremonti, C. A., Heckman, T. M., Kauffmann, G., et al. 2004, ApJ, 613, 898
van der Burg, R. F. J., Muzzin, A., & Hoekstra, H. 2016, arXiv:1602.00002
van Dokkum, P. G., Abraham, R., Merritt, A., et al. 2015, ApJL, 798, L45
Vazdekis, A., Sánchez-Blázquez, P., Falcón-Barroso, J., et al. 2010, MNRAS, 404, 1639
Veilleux, S., & Osterbrock, D. E. 1987, ApJS, 63, 295
Vogt, F. P. A., Dopita, M. A., & Kewley, L. J. 2013, ApJ, 768, 151
Yan, R., Bundy, K., Law, D. R., et al. 2016a, arXiv:1607.08613
Yan, R., Tremonti, C., Bershady, M. A., et al. 2016b, AJ, 151, 8
York, D. G., Adelman, J., Anderson, J. E., Jr., et al. 2000, AJ, 120, 1579